The Coordination of Cu^{II} in Zeolites − Structure and Spectroscopic Properties

Annelies Delabie,[a] Kristine Pierloot,*[a] Marijke H. Groothaert,[b] Robert A. Schoonheydt,[b] and Luc G. Vanquickenborne[a]

Keywords: Zeolites / Copper / Ab initio calculations / Density functional calculations / ESR spectroscopy / UV/Vis spectroscopy / Heterogeneous catalysis

Zeolites loaded with transition metal ions are promising heterogeneous catalysts. Knowledge about the location and structure of the metal centers is of paramount importance for the understanding of the catalytic potential of these materials. In this work, the spectroscopic studies of the coordination of Cu^{II} in zeolite A, ZK4, X, Y and mordenite are reviewed. Experimentally, diffuse reflectance spectroscopy (DRS) and electron spin resonance (ESR) spectroscopy have been applied to study the coordination of Cu^{II} in zeolites. Ab initio calculations on model clusters, representing the Cu^{II} sites in zeolites, are used for the interpretation of the experimental data. The combination of experimental spectroscopic information with theoretical results leads to a new and profound insight into the Cu^{II}–zeolite interaction.

1. Introduction

Zeolites are inorganic crystalline materials characterized by a regular structure of channels and cages of molecular dimensions. Their structure is built from tetrahedral units (TO_4), consisting of a central atom (T) − mostly Si^{IV} − coordinated to four oxygen atoms. Other atoms, especially

[a] Department of Chemistry, University of Leuven
Celestijnenlaan 200F, 3001 Heverlee-Leuven, Belgium
Fax: (internat.) + 32-16/327992
E-mail: Kristin.Pierloot@chem.kuleuven.ac.be
[b] Center for Surface Chemistry and Catalysis, University of Leuven
Kasteel Arenberg 23, 3001 Heverlee-Leuven, Belgium

Annelies Delabie (left top) completed her PhD study with the thesis "Computational study of transition metal ions in zeolites: structure, spectroscopy and reactivity" at the division of Quantum Chemistry, University of Leuven, Belgium, in May 2001 under the supervision of Professor Kristine Pierloot. Presently, she is a postdoctoral research fellow of the Flemish Fund of Scientific Research at the University of Leuven. She is the author of 12 scientific papers.

Kristine Pierloot (right top) is a Professor at the Department of Chemistry, University of Leuven. She received her PhD in Leuven in 1985 under the supervision of Professor Luc Vanquickenborne. She teaches general chemistry and computational chemistry. Her main research interest is the application of ab initio methods for the study of spectroscopic and magnetic properties of systems containing transition metals.

Marijke H. Groothaert (left center) was born in Neerpelt, Belgium in 1975. In 1998 she received her M. S. degree from the Faculty of Agricultural and Applied Biological Sciences, Catholic University of Leuven, Belgium. Since 1998 she is a PhD student at the Center for Surface Chemistry and Catalysis under the supervision of Professor Robert A. Schoonheydt. Her research is concentrated on the coordination of transition metal ions in zeolites and combines spectroscopic techniques with computational methods.

Robert A. Schoonheydt (left bottom) received his M. S. degree in 1966 and his PhD in 1970, both under the supervision of Professor Jan B. Uytterhoeven at the Catholic University of Leuven, Belgium. After one year as a postdoc with Professor Jack H. Lunsford in the Chemistry Department of Texas A&M University, USA, he returned to the Catholic University of Leuven as a National Fund of Scientific Research researcher. He became full professor in 1989. His teaching responsibilities include physical chemistry, analytical chemistry, and general thermodynamics for engineering students at the Faculty of Agricultural and Applied Biological Sciences. His research is concentrated in three areas: (1) spectroscopy and chemistry of surface transition metal ions, (2) molecular organization on clay surfaces, (3) theoretical modeling of molecule-surface interactions. He has authored more than 170 scientific papers, and is the editor of the book "Developments in the theory of chemical reactivity and heterogeneous catalysis". Presently, he is secretary-general of AIPEA and dean of the Faculty of Agricultural and Applied Biological Sciences. He also serves on the editorial board of Microporous and Mesoporous Materials, Applied Clay Science and European Journal of Inorganic Chemistry.

Luc G. Vanquickenborne (right bottom) is a Professor of theoretical chemistry at the Department of Chemistry, University of Leuven. He received his PhD and Dr. Hab. in Leuven, where he teaches quantum chemistry, computational chemistry, and inorganic chemistry. His main research interests are in the application of computational methods in different areas of chemistry.

MICROREVIEWS: This feature introduces the readers to the authors' research through a concise overview of the selected topic. Reference to important work from others in the field is included.

  1434−1948/02/0303−0515 $ 17.50+.50/0

Al^{III}, but also P^{V}, Ga^{III} and even transition metal ions can replace the central Si^{IV}. The tetrahedral units are linked by sharing all the oxygen atoms, leading to a wide variety of materials, differing in framework structure and chemical composition.[1] In the case of microporous solids (with aperture diameters from ca. 3 to 14 Å) the largest two subclasses are the aluminosilicates and aluminophosphates (the latter also known as ALPOs). This review will only deal with aluminosilicate zeolites. Other recent reviews focus on transition metal ions in aluminophosphate molecular sieves.[2,3]

As each Al^{III} incorporated in the silicate framework leads to one excess negative charge, an equivalent amount of extra-framework cations must be introduced to neutralize the structure. These cations, mostly Na^{I}, K^{I} and Ca^{II}, are present inside the cages and channels of the zeolite together with intrazeolitic water. They are not covalently bound to the zeolite framework and can therefore easily be replaced by transition metal ions by conventional aqueous ion exchange. After dehydration, these transition metal ions become localized. They are dispersed over the large internal surface of the zeolite, coordinating to the framework oxygen atoms. The obtained metal coordination environment is often not saturated, which means that these ions can act as coordination centers for adsorbed molecules or as catalytically active sites. The microporous character of the zeolite material puts limits on the size and shape of the interacting molecules, and hence enables shape selective reactions. Alternatively, transition metal ions can also be encountered at framework positions (the T atoms) in zeolites. In this case, the transition metal ions are already incorporated during the synthesis of the zeolite by so-called isomorphous substitution.

This review deals with studies of Cu^{II} in the zeolite channels, acting as a charge-compensating ion. These Cu−zeolites have been studied extensively because they display high activities for the catalytic and photocatalytic decomposition of NO and N_2O forming N_2 and O_2.[4−15] Also the selective reduction of NO by NH_3 or hydrocarbons is catalyzed by Cu−zeolites.[16−19]

A prerequisite for a fundamental understanding of the catalytic potential of Cu−zeolites is the knowledge of the location (and accessibility), coordination and electronic structure of the Cu ions. However, the location and coordination of transition metal ions inside zeolites are still a matter of debate. For aluminum-rich zeolites, one usually assigns the cations to well-defined rings or cages in the zeolite structure. The preference of the cation for occupation of these specific extra-framework sites can be thought of as arising from favorable interactions between the cation and the framework structure. The study of the distribution of the transition metal ions throughout the zeolite is usually referred to as cation siting.[20−21] On the other hand, it has also been suggested that the location of cations, especially divalent cations, is determined by the distribution of aluminum in the zeolite lattice.[22−25] Indeed, it can be expected, on the basis of simple electrostatic considerations, that divalent cations are preferentially located in the proximity of two framework aluminum atoms. The importance of charge compensation by aluminum must be emphasized in particular in the case of Si-rich zeolites. Unfortunately, the exact positions of aluminum ions in the zeolite lattice are unknown, and there is no general agreement on whether the distribution of aluminium is random or ordered.

We intend to give an overview of the studies on the siting and coordination of Cu^{II} in zeolites by means of spectroscopic and theoretical methods. Especially diffuse reflectance spectroscopy (DRS) and electron spin resonance (ESR) spectroscopy have been applied extensively in the study of the coordination of Cu^{II} in zeolites. We will focus on Cu^{II} in zeolite A, ZK4, X, Y and mordenite because of their well-documented literature. The spectroscopic fingerprints of the Cu^{II} species in these zeolites are now firmly established, as shown in a previous review[20] in 1993. However, there is still a good deal of disagreement on the interpretation of the spectroscopic data. At the time of the 1993 review, the spectroscopic fingerprints were mainly interpreted from XRD results or by means of semi-empirical calculations. Recently, however, it has become possible to study the coordination and spectroscopic features of Cu^{II} in zeolites by means of ab initio calculations.[26−32] Large model clusters were constructed, representing the possible Cu^{II} sites in the different zeolites. The structure of the Cu^{II} coordination environment was obtained from geometry optimizations based on density functional theory (DFT). Multiconfigurational perturbation theory (CASPT2) was used for the calculation of the spectroscopic features of these clusters. As will be shown in the present review, the combination of these ab initio results with the available experimental spectroscopic information is a powerful research tool, and leads to new and detailed information on the interaction of Cu^{II} with zeolites. We therefore present a summary of the new ab initio results and compare them with the older methods and interpretations.

We note that the present review will be limited to "model materials", i.e. with high Al contents (Si/Al ratio between 1 and 5) and with low Cu^{II} contents. Isolated and bare Cu^{II} sites are then present in the fully dehydrated state. Spectroscopic techniques clearly point to a limited number of well-defined Cu^{II} coordination modes in these zeolites, and the fingerprints can often be individually resolved, thereby facilitating the comparison with the ab initio results. On the other hand, several zeolites studied for catalytic processes contain Cu^{II} in larger than stoichiometric amounts. These so-called "overexchanged" zeolites do not only contain isolated Cu^{II} ions, but also Cu dimers or oxides. We have also incorporated some ab initio results for zeolite Y where the adsorption of one molecule (H_2O or NH_3) on the Cu^{II} site is studied.

The text is organized as follows: First, we recall the framework structures of zeolite A, faujasite and mordenite, together with a description of their most important cation sites. Next, we describe some of the major advantages and drawbacks of the spectroscopic techniques frequently used for the study of Cu^{II} in zeolites, mainly X-ray diffraction (XRD), diffuse reflectance spectroscopy and electron spin

resonance spectroscopy. We also discuss why theoretical calculations can be useful for the interpretation of the spectroscopic information. Finally, we present a critical overview of both experimental and theoretical spectroscopic studies of Cu^{II}−zeolites.

2. Overview of Zeolite Structures and Cation Sites

2.1 Zeolite A, ZK4, X and Y

The structure of zeolites with LTA (e.g. zeolite A, ZK4) or FAU topology (e.g. zeolite X, Y) can be visualized as a regular stacking of sodalite cages. The sodalite unit comprises 24 T atoms that make up a truncated octahedron, and 36 bridging oxygen atoms. Usually, the structure of a zeolite framework is represented in a schematic way. As shown in Figure 1, the vertices give the position of the T atoms, while the lines connecting the vertices represent the oxygen atoms.

One can see in Figure 1A that in zeolite A, the sodalite cages are connected through the oxygen four-membered rings. They enclose a larger volume, the supercage, with eight-membered ring apertures. The contours of this supercage are indicated in Figure 1A by dashed lines. The Si/Al ratio of zeolite A is 1, implying a strict alternation of Si and Al tetrahedra according to the Loewenstein rule.[33] ZK4 has the same topology as zeolite A, but a higher Si/Al ratio.

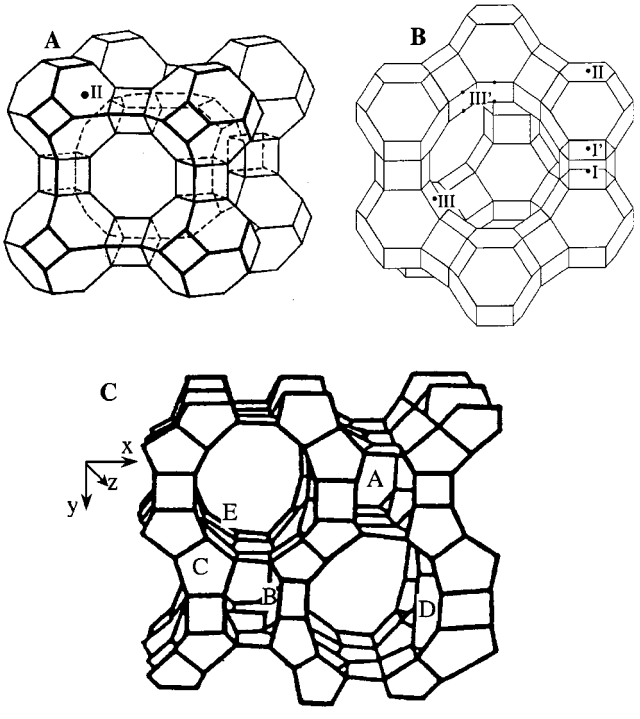

Figure 1. Schematic framework structure of zeolite A, ZK4 (A), zeolite X, Y (B) and mordenite (C); only the T atoms are shown on the vertices of the structure, the oxygen atoms are arranged in between; the location of the exchangeable cation sites is also indicated; the contours of the supercage in zeolite A are shown by dashed lines

For zeolite A and ZK4, only one site for Cu^{II} has been proposed: It is indicated as site II in Figure 1, at the oxygen six-membered ring between sodalite and supercage. The atomic structure of this six-membered ring is shown in Figure 2. This cation site has C_{3v} symmetry. One can see that there are six oxygen atoms available for coordination with the Cu^{II} ion. Three of them (indicated with O_A) are bent slightly inwards, and are therefore favorably located for coordination with a cation in the ring. The other three oxygen atoms (O_B) are bent outwards and therefore seem less accessible.

On the other hand, the sodalite cages can also be linked via the six-membered rings to form hexagonal prisms, as for the faujasite (FAU) topology (see Figure 1B). The interior supercage can be entered via twelve-membered rings, and is therefore much larger than the supercage of zeolite A. Zeolite X and Y are both members of the faujasite topology;

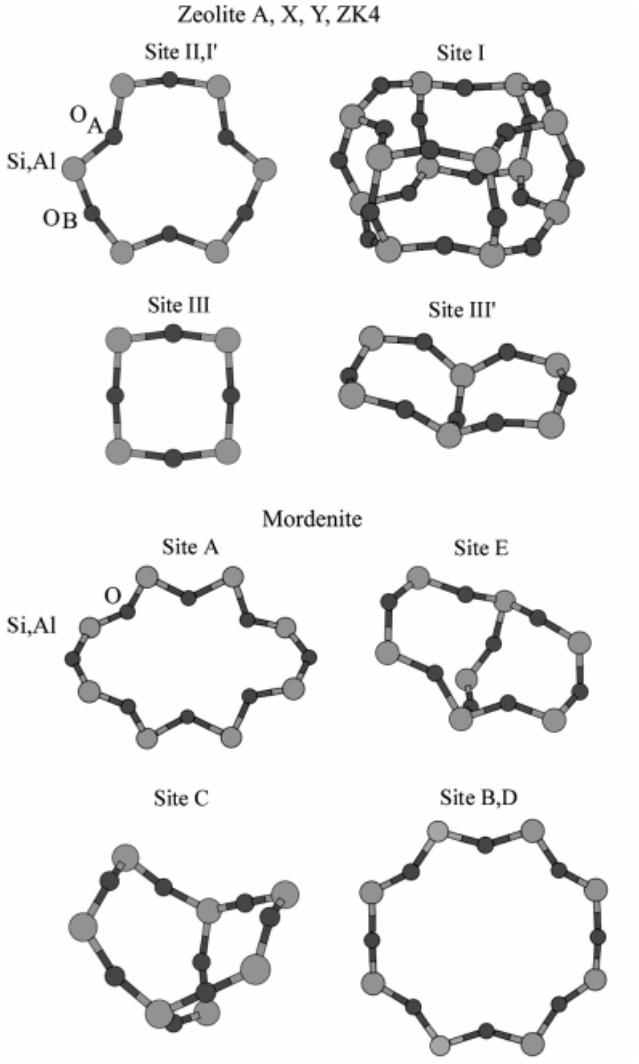

Figure 2. The common cation exchange sites of zeolite A and ZK4 (site II), X and Y (sites II, I′, I, III, III′) and mordenite (site A, E, C, B and D); the two types of oxygen atoms in sites II and I′ are labeled as O_A and O_B

they differ only by the aluminum content. Zeolite X has an Si/Al ratio between 1 and 1.25; faujasites with an Si/Al ratio higher than about 2 are generally referred to as zeolite Y.

As shown in Figures 1 and 2, many possible cation sites are present in the faujasite structure. Due to the tetragonal stacking of the sodalite cages, one can distinguish two distinct types of six-membered ring sites in faujasite. In Figure 2, these two types of six-membered rings are represented in the same picture, as they differ only by the zeolite surroundings extending beyond the atoms on display. One can, however, clearly see in Figure 1 that site II is the hexagonal window between the sodalite cage and the supercage, and it is therefore similar to site II in zeolite A. On the other hand, site I′ is one of the base planes of the hexagonal prism. A completely different cation site is the center of the hexagonal prism (site I), where the cations may obtain a sixfold coordination by binding with the three O_A oxygen atoms of the two six-membered ring base planes. Finally, cations may coordinate to oxygen atoms of the four-membered ring structures III and III′, located at the walls of the supercage.

2.2 Mordenite

Mordenite (MOR) is one of the pentasil zeolites. In these zeolites, five-membered ring building units (the pentasil units) are linked to form parallel columns. In the complex framework of mordenite (see Figure 1C), these columns are arranged along the *z* direction, so that they enclose a large, straight twelve-membered ring channel along the *z* direction, often referred to as the main channel, and eight-membered ring side-pockets. There is also an eight-membered ring zigzag channel, but as it runs in a direction perpendicular to the main channel, this channel is not visible in Figure 1C. The Si/Al ratio in the pentasil zeolites is usually considerably higher than in zeolite A and faujasite. The typical Si/Al ratio of mordenite is 5, but structures with higher Si/Al ratios can be synthesized.

The location of the cation sites in the mordenite structure is also indicated in Figure 1C, while the detailed structures of the sites can be seen in Figure 2. A first cation site in mordenite is site A, a twisted eight-membered ring located in the eight-membered ring side-pockets. The symmetry of this site is C_{2h}. The six most central oxygen atoms can coordinate with cations in this site. The E site is the planar six-membered ring in the twelve-membered ring channel. This six-membered ring is significantly different from the trigonal six-membered ring sites encountered in zeolite A and Y because it is formed by connecting two (bent) five-membered rings (see Figure 2). As a consequence, even an ideal E site in mordenite shows only C_s symmetry, whereas the highest possible symmetry of the six-membered ring sites in zeolite A and Y is C_{3v}. Cations in site E usually coordinate to the four central oxygen atoms of the six-membered ring. Other cation sites in mordenite are site D, the circular eight-membered rings situated at the walls of the large twelve-membered ring channel, and site B, a similar eight-membered ring in the side-pockets. There is also a boat-shaped site in the eight-membered ring channel of the zeolite; the latter site is composed of a non-planar six-membered ring (site C) in between two five-membered rings. As one can see from Figure 2, this six-membered ring also contains, like site E, an O−T−O bridge. The corresponding planar five-membered ring leads to the main channel of mordenite. It is not known which cation coordination environments can be achieved in site C. One can see from Figure 2 that site E and site C have the same topology, but a different shape.

3. Experimental and Theoretical Tools

3.1 Electron Spin Resonance

The first studies of the coordination of Cu^{II} in zeolites, starting from the year 1959, were based on ESR.[34,35] The ESR spectrum is very sensitive to the surroundings of the Cu^{II} ion, as manifested by the *g* tensor and the hyperfine splitting. The number of ESR signals present in the spectrum therefore indicates the number of different coordination environments of Cu^{II}. The initial goal of the ESR studies of Cu^{II}−zeolites was to draw conclusions concerning the coordination environment of Cu^{II} in unknown zeolite surroundings by comparing ESR spectroscopy data with that of Cu^{II} in crystals of known structure. However, since the ESR spectra turn out to be very sensitive to the degree of hydration, the temperature of the heat treatment during dehydration and the nature of other cations in the zeolite, the early reported ESR spectral parameters varied strongly from one report to another.[34−42] Over the years, a consensus emerged in the literature on the ESR parameters of the fully dehydrated Cu^{II}−zeolites, which are by now firmly established.[20] On the other hand, the interpretation of this spectroscopic information is not straightforward. One has attempted to obtain more information about the accessibility of the Cu^{II} species by studying the dependence of the ESR signal on the adsorption of small molecules on the Cu^{II} sites and on the degree of dehydration of the Cu^{II}−zeolite.

Additionally, the pulsed electron spin resonance technique called electron spin-echo (ESE) spectroscopy can measure the superhyperfine interaction between the Cu^{II} ion and nearby magnetic nuclei (for example ^{27}Al).[43] These very weak hyperfine interactions cannot be observed in a conventional ESR spectroscopy experiment, but they show up as a modulation of the decay of the time domain ESE spectrum. By proper analysis of this modulation one can determine the types, number and distances of magnetic nuclei surrounding the Cu^{II} ion.

In order to avoid magnetic dipole interactions between different Cu^{II} centers, the ESR spectra are recorded at low Cu^{II} exchange levels.[44]

3.2 Diffuse Reflectance Spectroscopy

Diffuse reflectance spectroscopy (DRS) allows the measurement of the electronic transitions in the UV/Vis/NIR region from a powdered zeolite sample. As the excitation en-

ergies of the transitions within the 3d shell depend on the ligand field surrounding of the transition metal ion, these spectra provide a "fingerprint" of the local Cu^{II} coordination environment in the considered zeolite. In many cases, however, not one but several different coordination environments are present inside the zeolite. Hence overlapping spectra are obtained, and the spectrum must be deconvoluted into its individual components.[45−48] DRS spectra are therefore often measured at low exchange levels, as it is assumed that under low load conditions only the preferential coordination sites are occupied.

ESR and DRS both have the advantage that, although their spectra may represent a superposition of several Cu^{II} coordinations, the local atomic environments of Cu^{II} can often be extracted from progressive loading and preferential site occupations.

3.3 X-ray Diffraction

X-ray diffraction (XRD) is the most direct method of obtaining the location of the exchangeable cations in the zeolite unit cell. However, a major limitation of XRD in the study of transition metal exchanged zeolites is that no distinction can be made between Si and Al in the lattice. The apparent symmetry of the coordination environment of cations obtained with XRD is therefore often too high. This means that the local effect of Al on the coordination environment of the cation cannot be investigated with XRD. Another disadvantage is that in the case of partial site occupancy XRD visualizes only an average structure for the given crystallographic site, whether it is occupied or empty. Hence, XRD as such provides only average information, pertaining to the overall structural integrity, as opposed to ESR and DRS, which reveal the local atomic environment of the transition metal ion.

Apart from these disadvantages, there are also limits in the preparation of suitable samples. With high-alumina zeolites (such as zeolite A, X and Y), it is usually possible to obtain concentrations of divalent cations in the zeolite matrix which are sufficiently high to allow determination of their location in the zeolite unit cell. However, with siliceous zeolites, levels of exchange are low. Since the unit cell of such zeolites is often large and has low symmetry, the limited number of available metal ions is distributed among several crystallographically different positions.

Ever since the first XRD study of Cu^{II} zeolite Y, the XRD structures of Cu^{II}−zeolites have been used to interpret the ESR signals and DRS spectra.[49] One should, however, be careful with such a comparison, not only because XRD reports only average Cu^{II} coordination environments, but also because the XRD results are reported for highly loaded Cu^{II} samples (close to complete exchange), while in ESR and DRS often zeolites with low Cu^{II} contents are studied.

3.4 Theoretical Calculations

Even the combination of complementary experimental techniques cannot always provide a conclusive picture of the siting of Cu^{II} ions in zeolites. As one will see from the literature overview in sections 4 and 5, different authors have proposed different sites for Cu^{II} in zeolites. In order to obtain a sound interpretation of the spectroscopic data, at the end of the 1970s Klier started to perform theoretical calculations.[50−52] He carried out semi-empirical calculations on a simple CuO_3 model to study the electronic structure of Cu^{II} in the trigonal six-membered ring site of zeolite Y, and proposed the first assignment of the ligand field bands measured by DRS. The group of Schoonheydt soon followed this example and studied the spectroscopic properties of Cu^{II} at several exchange sites (in zeolite Y, mordenite), with calculations based on the angular overlap model (AOM).[20,53−55] These theoretical results were used to provide an interpretation for the available ESR and DRS data. One disadvantage was that the only structural information available was obtained from XRD. These calculations were therefore performed at the average XRD structures.

Thanks to the rapid development of computer power, today it has become possible to perform ab initio calculations on model clusters large enough to represent the cation exchange sites in zeolites. Pierloot et al. have studied the coordination of Cu^{II} in various zeolites (zeolite A, Y, ZK4 and mordenite) with a cluster model approach.[26−32] The considered clusters include the Cu^{II} ion surrounded by a zeolite ring (or a combination of rings), terminated by either OH groups or hydrogen atoms. The structures of the cluster models were obtained from partial geometry optimizations, based on density functional theory (DFT). The spectroscopic features (ligand field excitation energies and ESR g factors) were calculated by means of the CASPT2 method, i.e. multiconfigurational perturbation theory. The calculated results were compared with the experimental DRS and ESR spectra. This comparison allowed detailed information about the Cu^{II} coordination in zeolites to be obtained. The present approach was also applied to study the coordination of Co^{II} in the six-membered ring sites in zeolites.[26,56] The main features of the electronic spectrum of Co^{II} in zeolite A and Y are successfully described.

We note that very recently Larsen et al. used DFT to calculate both ESR g values and A values of several vanadyl model complexes, in which H_2O molecules were used to represent the framework oxygen atoms.[57] Theory and experimental results were also combined here, but this time to interpret the ESR spectra of VO^{2+}-exchanged zeolites.

Another theoretical approach has been followed by Sauer and co-workers.[58−60] A combined quantum mechanics/interatomic potential function technique was developed, in which the cation exchange site is treated by quantum mechanical methods, while the periodic lattice is treated by an ion pair shell model potential. Using this method, the location, structure and coordination of isolated Cu^{I} ions in ZSM-5 were studied.[61,62] Photoluminescence energies of Cu^{I} sites were also calculated, and could help in assigning the observed bands of the Cu^{I} luminescence spectra.

We have also noted that during the last years, many other ab initio studies have concentrated on the catalytic potential of Cu-containing zeolites.[59,61−77] Various kinds of cluster

models have been constructed in order to represent the Cu^{II} coordination in the zeolite. There is, however, still no agreement about the active site and reaction mechanism of − for instance − the decomposition reactions of NO and N_2O.

3.5 Additional Observations

Although the previous techniques are most often used in order to probe the coordination environment of Cu^{II} in zeolites, other experimental techniques provide complementary information. Infrared spectroscopy of adsorption complexes in Cu−zeolites (mostly of NO and CO) is often used as a selective probe for Cu ions because there is a shift in the vibration frequencies depending on the copper oxidation state and its coordination environment. The technique can therefore be used to discriminate between different Cu sites.[23,78] Secondly, IR measurements have shown that cations induce local perturbations of the T−O−T bonds adjacent to the cation, reflected in a shift of the skeletal T−O−T vibrations.[79,80]

Determination of the Cu oxidation state, coordination number and Cu−O bond lengths can be achieved by X-ray absorption fine structure (XAFS) techniques.[81,82] However, for isolated Cu^{II} sites the EXAFS (extended X-ray absorption fine structure) spectrum only yields average Cu−O bond lengths and coordination numbers. Hence, this technique is not well suited to offer detailed information on the different Cu^{II} sites and is more often used to distinguish between isolated versus clustered Cu ions in over-exchanged zeolites.

The photoluminescence spectra of Cu^{I} ions are highly sensitive to their coordination environment. The $Cu^{I}(3d^{9}4s^{1})-Cu^{I}(3d^{10})$ transition energies have been measured by several groups for several zeolites. The group of Wichterlová started from the assumption that the Cu ions do not migrate upon reduction of Cu^{II} to Cu^{I}. Therefore they use the various bands in the luminescence spectra of Cu^{I} zeolites to distinguish between different types of Cu^{II}.[23−25]

Few NMR spectroscopic studies have been reported for studying the coordination of cations inside zeolites. They are based on ^{65}Cu NMR[83] or ^{129}Xe NMR spectra of Xenon adsorbed in various Cu−zeolite samples. Due to the large polarizability of the latter ion, its chemical shift is very sensitive to its environment.[84−86]

4. Cu^{II} in Zeolites A, ZK4, X and Y

Below, we present a literature overview of the spectroscopic and theoretical studies of Cu^{II} zeolites. Because of their related framework structures, zeolite A, ZK4, X and Y are treated together. The XRD results of Cu^{II}−zeolites will be discussed before the results of the spectroscopic studies (ESR and DRS), since they may give a first indication of the possible Cu^{II} sites in the zeolites. Next, the results of the ab initio calculations are summarized and compared with the earlier interpretations.

4.1 Diffraction Studies

The structure of fully exchanged Cu^{II} zeolite A was determined by single-crystal XRD in the cubic space group *Pm3m*.[87] All Cu^{II} ions are located in site II, on the threefold axes in the hexagonal six-membered rings. The coordination environment of Cu^{II} in this site is shown in Figure 3. The Cu^{II} ion is coordinated to three close-by oxygen atoms (O_A), at a distance of 2.14 Å. A second shell of three oxygen atoms is found at a distance of 2.85 Å from Cu^{II}. The Cu^{II} ion extends slightly into the large cavity, giving rise to an O_A-Cu-O_A angle of 119°.

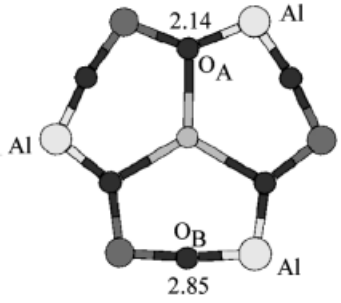

Figure 3. Trigonal coordination environment of Cu^{II} in the six-membered ring site II of zeolite A, as obtained from XRD;[87] Cu−O distances are given in Å; the labeling of the two types of oxygen atoms (O_A and O_B) is also indicated

On the other hand, XRD reveals several exchange sites for Cu^{II} in zeolite Y. Two XRD studies on $Cu^{II}-Y$ have indicated that the six-membered rings are the favored, although not the only possible cation sites for Cu^{II}. First, an X-ray powder diffraction study of a 50% exchanged $Cu^{II}-Y$,[49] reported that Cu^{II} ions are, for the most part, present in six-membered ring site I′. The large affinity of Cu^{II} for site I′ was ascribed to the opportunity to be firmly bound to three O_A atoms of the zeolite framework. The remaining Cu^{II} ions were located at the center of the hexagonal prism (site I) in an octahedral coordination environment.

Secondly, a single-crystal XRD experiment on a 90% exchanged $Cu^{II}-Y$ by Maxwell and de Boer[88] pointed to the presence of Cu^{II} ions in both six-membered rings I′ and II. The coordination environment is trigonal; the Cu−O distances are compared with the other XRD structures in Table 1. Only a very small fraction of the Cu^{II} ions were found in the hexagonal prism I, in a sixfold coordination environment. Finally, Cu^{II} ions were also found in the four-membered ring sites III and III′.

Table 1. Cu−O distances (given in Å) in the trigonal six-membered ring sites, obtained from X-ray diffraction studies on $Cu^{II}-A$ and $Cu^{II}-Y$

Zeolite	Site	$Cu-O_A$	$Cu-O_B$
$Cu^{II}-A$[87]	II	2.14	2.85
$Cu^{II}-Y$[49]	I′	2.00	2.91
$Cu^{II}-Y$[88]	II	2.22	2.92
	I′	2.12	2.95

Recently, a pulsed-neutron diffraction study of solid-state copper(II)-exchanged zeolite Y (with a Cu-exchange level of 87%) was also reported.[89] This study indicated that Cu^{II} occupies three sites. About half of the Cu^{II} ions were found in site III′, each coordinated in a near square-planar manner to four framework oxygen atoms. However, an undetected fifth ligand (H_2O, OH^- or Cl^-) may be present, coordinating axially to Cu^{II} so as to give a distorted square pyramid. 31% of Cu^{II} are placed at site I′ in a trigonal coordination with Cu−O distances of 2.17 Å. The remaining Cu^{II} ions are present in site I.

4.2 ESR Spectroscopic Results

Zeolite A and ZK4

In the first ESR studies of Cu^{II} in zeolite A no agreement was reached on the number of Cu^{II} species or the characteristic ESR parameters of these species.[90−92] Most of the later studies agree that only one axially symmetric signal is present in the ESR spectrum of fully dehydrated Cu^{II} zeolite A, described by $g_{//}$ = 2.37−2.41 (see Table 2).[20,28,53−55,93,94] The presence of one ESR signal is in good agreement with the XRD study, pointing to Cu^{II} at only one site, the trigonal six-membered ring II.[87] Kevan et al.[93−96] monitored the coordination of Cu^{II} in zeolite A during the process of dehydration by electron spin echo spectrometry. After complete dehydration, they described the Cu^{II} coordination as close to the plane of the six-membered ring site II, in a position displaced 0.2 Å into the supercage, where it is trigonally coordinated to three of the six lattice oxygen atoms. This coordination environment is very similar to that obtained by XRD (see Figure 3).

The coordination of Cu^{II} in ZK4 has also been studied. Two Cu^{II} species were detected by ESR spectroscopy, characterized by $g_{//}$ = 2.357 and 2.321.[97] The former signal was assigned to Cu^{II} in the six-membered ring site II, moved inside the sodalite cage, while the latter signal was attributed to Cu^{II} ions at the same site, but extended into the supercage. The presence of these two ESR signals in Cu^{II}−ZK4 was recently confirmed.[28] However, a totally different interpretation based on ab initio calculations was given, as will be detailed in section 4.4.

Table 2. An overview of the ESR parameters found in literature of Cu^{II} in various zeolites; for references, see text

Zeolite	$g_{//}$	$g_{\perp}$
Cu^{II}−zeolite A	2.37−2.41	2.06−2.07
Cu^{II}−ZK4	2.36	2.07
	2.32	2.07
Cu^{II}−zeolite Y	2.36−2.41	2.07−2.08
	2.30−2.34	2.05−2.07
Cu^{II}−zeolite X	2.37−2.38	2.06
	2.35	2.06
Cu^{II}−mordenite	2.32−2.34	2.05−2.06
	2.27−2.29	2.05−2.06

Zeolite Y and X

Most authors report at least two overlapping axial signals in Cu^{II}−zeolite Y.[20,28,36−42,53−55,86,92−94,98−103] Generally, there is agreement about the parameters describing these ESR spectra (see Table 2). One of the signals conforms to the one observed in zeolite A with $g_{//}^{(1)}$ = 2.36−2.41. The second signal is characterized by a much smaller $g_{//}$ value, $g_{//}^{(2)}$ = 2.30−2.34. It was suggested that these ESR signals are, within experimental accuracy, independent of the Si/Al ratio, the Si−Al ordering and the type of co-exchanged cation.[20,53] As such, they only reflect the type of coordination of Cu^{II} in the structure. However, the relative intensities of the two ESR signals vary with the Si/Al ratio, the type of co-cation and the Cu^{II} loading, and are indicative of the site preference of Cu^{II}.[20,53]

Interpretations of the two ESR signals of Cu^{II} in zeolite Y in terms of specific coordination environments at cation sites were published only after the first XRD study of Cu^{II}−Y became available. Almost all groups assign the two ESR signals to Cu^{II} at two different cation sites. However, different research groups have proposed different sites for Cu^{II}. Conesa and Soria[102,104−106] suggested that Cu^{II} remains mainly in the two types of trigonal six-membered rings in the final dehydrated state, at positions I′ and II. This interpretation is in agreement with subsequent studies by Herman[92] and Schoonheydt,[20] and was also confirmed by O_2 line-broadening experiments. The O_2 molecule can only enter the large supercage of zeolite Y, but it cannot access the smaller sodalite cages and hexagonal prisms (see also Figure 1B). One can therefore expect that the ESR signals of Cu^{II} in the supercage (site II, III, III′) will be broadened by the dipolar interaction between the O_2 molecule and Cu^{II} (the resolution and signal intensity decrease), while the ESR signals of Cu^{II} in the sodalite cage and hexagonal prism (site I, I′) are not affected. Since the ESR signal with $g_{//}^{(1)}$ = 2.38 disappears upon admission of oxygen, it was assigned to Cu^{II} in six-membered ring site II in the supercage, with Cu^{II} in a distorted trigonal coordination environment. This assignment also seems very reasonable, because of the similarity of the parameters of this signal with those of the Cu^{II} ions encountered in zeolite A, where the Cu^{II} ions are also present in site II. On the other hand, the signal with $g_{//}^{(2)}$ = 2.33 is insensitive to the presence of oxygen molecules and was assigned to Cu^{II} ions in site I′. As the latter ESR parameters are characteristic for a square-pyramidal coordination, Conesa and Soria suggested that the Cu^{II} ions in site I′ should remain coordinated to two water molecules in order to realize such a coordination.[106] On the other hand, Schoonheydt assigned this signal to naked Cu^{II} ions in site I′ in a trigonal coordination environment.[20] We will come back to this point in section 4.4.

In the Cu^{II}−zeolite X, two axial ESR signals are also observed.[20,36,42,107−110] A first signal conforms to the one observed in both zeolite A and Y, and is characterized by $g_{//}^{(1)}$ = 2.37−2.38. The second is described by a somewhat higher $g_{//}^{(2)}$ value than the second signal in zeolite Y, 2.35

instead of 2.30−2.34. Schoonheydt assigned the signal with $g_{//}^{(1)} = 2.37-2.38$ in zeolite X to Cu^{II} ions in site II, in line with the assignments of Cu^{II} zeolite A and Y. On the other hand, the second signal in Cu^{II}−X was assigned to a different site; since this ESR signal is also broadened by O_2, it was assigned to the Cu^{II} ions in the supercage at site III′.

A different site-dependent interpretation of the ESR signals in zeolite Y and X was provided by the group of Kevan, who used ESR spectroscopy in combination with electron spin echo (ESE) spectrometry.[21,97,103,109−113] These authors propose the same sites for Cu^{II} in zeolite X and Y. The ESR signal with $g_{//}^{(1)} = 2.39$ was attributed to an almost planar trigonal Cu^{II} coordination in the six-membered ring site I′ of zeolites X and Y. On the other hand, the signals with $g_{//}^{(2)} = 2.33$ and $g_{//}^{(2)} = 2.35$ in zeolite Y and X, respectively, were suggested to both correspond to Cu^{II} in the hexagonal prism I. This assignment is in agreement with the earliest XRD results[49] and with the findings of Iwamoto,[114] who studied the oxygen adsorption in Cu^{II}−zeolites Y by temperature-programmed desorption (TPD).

Matar and Goldfarb studied the interactions of the Cu^{II} cations with framework Al in zeolites A, X and Y in various stages of dehydration and after methanol adsorption by electron spin echo envelope modulation (ESEEM).[115−117] The spectra show contributions from two types of ^{27}Al nuclei. One type includes first-shell Al, bound to the oxygen atoms to which the Cu^{II} ion is coordinated; they are at about 3.1−3.4 Å from the Cu^{II} ion and exhibit relatively large isotropic hyperfine constants which indicate strong interaction with the framework oxygen atoms. The second type consists of distant Al nuclei, situated at distances larger than 5 Å. Orientation-selective ESEEM experiments provide additional structural information: The modulation of the first-shell Al in some cases showed strong orientation dependence. Based on these results, a link was proposed between the ESR $g_{//}$ values of the coordinated Cu^{II} and the position of this ion with respect to the aluminum atoms in the trigonal six-membered ring. The Cu^{II} ions situated close to a plane of Al nuclei are held responsible for the $g_{//}$ value of 2.33, whereas the larger $g_{//}$ value (2.38) is supposed to originate from Cu^{II} ions located away from the plane of Al nuclei. This interpretation is original in its suggestion that the different ESR signals might actually be due to Cu^{II} at one and the same site, but surrounded by different Al distributions. A somewhat similar idea will be backed by ab initio calculations (section 4.4), where it is shown that the ESR signals can indeed be explained by Cu^{II} in the six-membered ring site with different Al surroundings.

4.3 DRS and Ligand Field Theory

Klier was the first to interpret the diffuse reflectance spectrum of dehydrated Cu^{II}−zeolite Y.[50−52] This spectrum is composed of a narrow peak centered at 10900 cm^{-1} and two broader bands centered at 12700 and 14650 cm^{-1}. He studied the electronic structure of Cu^{II} positioned in the six-membered ring site, represented by a CuO_3 model. The presence of one hole in its 3d shell corresponds to the free $Cu^{II}(d^9)$ ion in a ^2D ground state. The C_{3v} symmetry of the oxygen environment imposes a splitting on the Cu^{II} ^2D ion term as shown in Figure 4A. The ground state is a degenerate ^2E, with the one hole in the 3d shell located in the e shell, consisting (to a first approximation) of the $3d_{x^2-y^2}$, $3d_{xy}$ orbitals. The Jahn−Teller effect was invoked, inducing an off-axial distortion to remove this degeneracy, as also shown in Figure 4A. Furthermore, the effect of spin-orbit coupling was considered. By fitting the energy of the three highest transitions to the experimental band positions, the Jahn−Teller coupling constant *b*, the spin-orbit coupling constant λ, and β, a structural parameter, were determined. As such, an O−Cu−O angle of 117° was determined, in (somewhat fortuitous) agreement with the angle found by XRD (of 115°). This means that the Cu^{II} ion would obtain an almost planar coordination in the six-membered ring. Klier's assignment of the ligand field transitions is presented in Table 3.

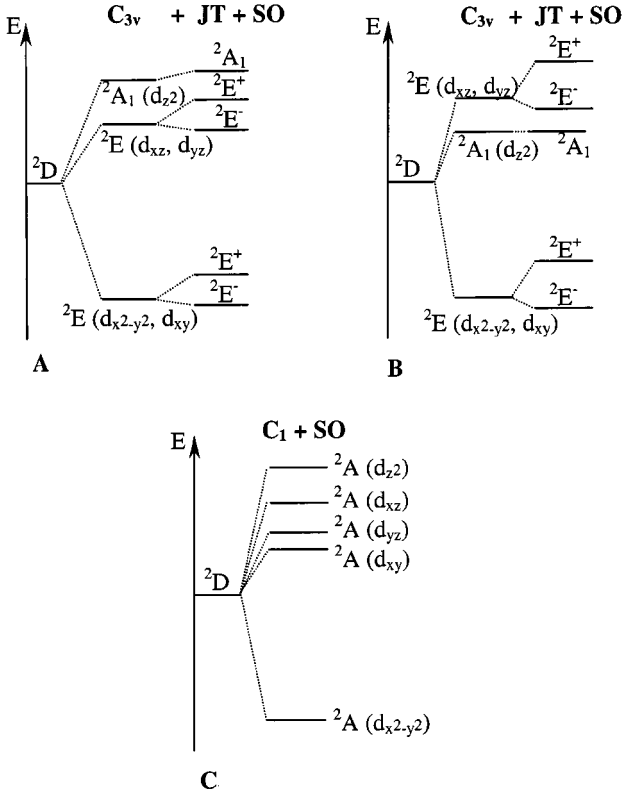

Figure 4. Energy term diagram for Cu^{II} in the trigonal six-membered ring site of zeolite A, ZK4, X, Y by Klier (A),[51] Schoonheydt (B)[53] and Pierloot (C)[28]

Table 3. Assignments of the ligand field bands of Cu^{II} in the trigonal six-membered ring site by various authors

Band maximum [cm^{-1}]	Assignments		
	Klier	Schoonheydt	Pierloot
10900	$^2E_1 \rightarrow {}^2E_2^-$	$^2E_1 \rightarrow {}^2A_1$	$X^2A \rightarrow b^2A$ $X^2A \rightarrow c^2A$
12700	$^2E_1 \rightarrow {}^2E_2^+$	$^2E_1 \rightarrow {}^2E_2^-$	$X^2A \rightarrow d^2A$
14650	$^2E_1 \rightarrow {}^2A_1$	$^2E_1 \rightarrow {}^2E_2^+$	$X^2A \rightarrow e^2A$

Packet and Schoonheydt[20,53−55] studied the coordination of Cu^{II} in various zeolites by combined DRS/ESR experiments. The ligand field band positions for Cu^{II} in zeolite A, X and Y are summarized in Table 4. As one can see, these spectra all show ligand field transitions at similar energies. In contrast to the ESR results, no pronounced difference is found between the DRS spectra of Cu^{II}−A on the one hand and Cu^{II}−X and −Y on the other hand. As already explained in section 4.2, the Cu^{II} ions were assigned to site II and I′ for zeolite Y, while sites II and III were proposed for Cu^{II} in zeolite X. These assignments were supported by calculations based on the angular overlap model (AOM).[20,53−55] Schoonheydt et al. further extended the work on the CuO_3 complex of Klier by also including the three more distant oxygen atoms of the six-membered ring. The two types of six-membered ring sites of zeolite Y, site I′ and II, were both considered. Not only were the three ligand field bands calculated but also the ESR parameters $g_{//}$, $A_{//}$ and $g_{\perp}$. In agreement with Klier, a distortion of the trigonal geometry of the six-membered rings was proposed, due to a Jahn−Teller effect. Spin-orbit coupling was taken into account. By the least-squares procedure, the values of six adjustable parameters were then optimized, the AOM spectroscopic parameters σ and π, a geometrical parameter, the Jahn−Teller parameter, the spin-orbit coupling constant and the Fermi contact parameter. The resulting assignment of the ligand field spectrum is compared to that of Klier in Figure 4 and Table 3. As one can see, the sequence of the $^2A_1$ and ^2E terms is reversed. The reason can be traced back to a different value for the π/σ ratio from both authors. The ligand field stabilization energy of Cu^{II} in site I′ and II was calculated. From these calculations, no site preference between type I′ and II six-membered rings could be predicted.

Both Klier and Packet obtained rather unusual values for the spectroscopic parameters from their ligand field calculations. The spectra of Klier were calculated at an extremely high π/σ ratio, while Packet reports a very large σ value. The origin of these unrealistic parameters may be because the semi-empirical calculations started from the average XRD structures of Cu^{II} sites and are therefore performed in fictitious high symmetry coordination environments. The possibility of symmetry reduction, for example by an asymmetric aluminum surrounding, was not considered. As was suggested by Goldfarb[115−117] and will also be shown in the following section, this factor does play a crucial role in the Cu^{II}−zeolite interaction.

Table 4. Overview of DRS band positions of Cu^{II} in various zeolites by Schoonheydt et al.[20]

Zeolite	Band I	Band II	Band III
Cu^{II}−zeolite A	10400	12200−12800	15000−15400
Cu^{II}−zeolite Y	10400−10800	12400−13000	14700−15100
Cu^{II}−zeolite X	10400−11100	12400−13000	14700−15100
Cu^{II}−mordenite	12500	13700	14800

4.4 Ab initio Studies of Cu^{II} in Trigonal Six-Membered Ring Sites

Recently, more advanced quantum chemical calculations have been performed in order to investigate the coordination and spectroscopic properties of Cu^{II} in the trigonal six-membered ring site.[27−29] The results point to a new interpretation of the ESR signals in zeolite A and Y. Ab initio calculations were performed on the cluster models shown in Figure 5. They consist of the Cu^{II} ion in the six-membered ring, with OH groups (Figure 5A, denoted as "large models") or hydrogen atoms (Figure 5B, denoted as "small models") inserted in order to saturate the dangling bonds of Si, Al. The cluster models are thus represented by the structural formula $CuO_6Si_{6-x}Al_x(OH)_{12}^{(2-x)+}$ and $CuO_6Si_{6-x}Al_xH_{12}^{(2-x)+}$. Different aluminum contents and distributions were studied in order to examine the local effect of aluminum on the coordination environment and the spectroscopic properties of Cu^{II} in the six-membered ring.

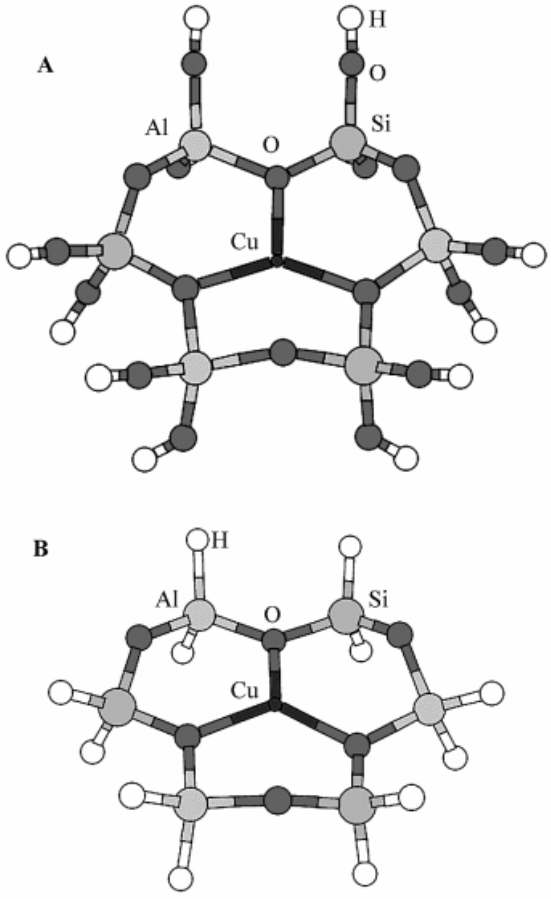

Figure 5. Cluster models for the ab initio calculations of Cu^{II} in the trigonal six-membered ring site in zeolites A, ZK4, X and Y: (A) the dangling bonds of the silicon or aluminum atoms are terminated by OH groups ("large models"); (B) the dangling bonds of the silicon or aluminum atoms are terminated by hydrogen atoms ("small models"); the clusters are depicted at the XRD starting geometry as obtained from the literature[77]

The coordination environment of Cu^{II} in the six-membered ring was obtained by partial geometry optimizations of the large clusters (Figure 5A). The starting geometry of

the cluster models is based on XRD data of Cu^{II}−zeolite A.[87] Partial geometry optimizations of these cluster compounds were performed; restrictions were applied to mimic the rigidity of the zeolite framework. The geometry optimizations were based on density functional theory (DFT) with the B3LYP functional in combination with basis sets from Schäfer et al.[118] The accuracy of the obtained B3LYP-DFT structures was checked by performing additional restricted CASPT2 geometry optimizations for a few clusters.[28] Significant corrections were only obtained for the negatively charged $CuO_6Si_3Al_3(OH)_{12}^-$ cluster model.

As for the calculation of the electronic spectra and the *g* factors, calculations based on multiconfigurational perturbation theory (CASPT2) were performed. Since these CASPT2 calculations demand a considerably larger computational effort than the DFT geometry optimizations, slightly smaller models were used, obtained by replacing the terminal OH groups in the optimized cluster models by hydrogen atoms. It was shown that this reduction of the cluster size does not affect the spectroscopic features of the central Cu^{II} ion to any significant extent.[26,28] In the CASPT2 calculations, the basis sets are atomic natural orbitals.[119] The reference active space consists of the Cu(3d) orbitals, an additional d-shell (to take into account the 3d-double shell effect) and one bonding oxygen valence orbital. The effect of spin-orbit coupling was taken into account by means of an effective one-electron operator.[120] Finally, the *g* tensors were calculated using second-order perturbation theory, introducing spin-orbit coupling and the magnetic field as simultaneous perturbations. More information about the details of the calculations can be found in the original papers.[27−29]

First, it was checked whether the ligand field spectrum of Cu^{II}−zeolite A can be explained by assuming Cu^{II} to be coordinated in the high-symmetric (C_{3v}) oxygen six-membered ring structure as reported on the basis of XRD (see Figure 3). However, the CASPT2 excitation energies of a six-membered ring cluster at the XRD geometry did not exceed 8500 cm^{-1} for the ligand field transitions. Even after invoking a Jahn−Teller distortion, the calculated excitation energies remained much too low to offer an explanation of the experimental DRS spectra of Cu^{II}−A, −Y.

In a next step, the DFT-optimized structures of model clusters with all possible aluminum distributions in the six-membered ring were considered. All structures were optimized without applying any symmetry restrictions. The optimized coordination environments are shown in Figure 6. Only one Al is present in ring A, while rings B and C contain two, and ring D three Al. As one can see, the calculated structures reveal strong local deformations of the six-membered rings; as a matter of fact, no symmetry whatsoever is retained. The distortions are due to the tendency of the Cu^{II} ion to obtain a fourfold coordination environment in the six-membered ring. One of the more distant O_B oxygen atoms (O_{B1}) is bent inwards in order to provide an additional short Cu−O bond. This fourfold coordination environment gives rise to a much higher ligand field as compared to the trigonal coordination; the CASPT2 excitation

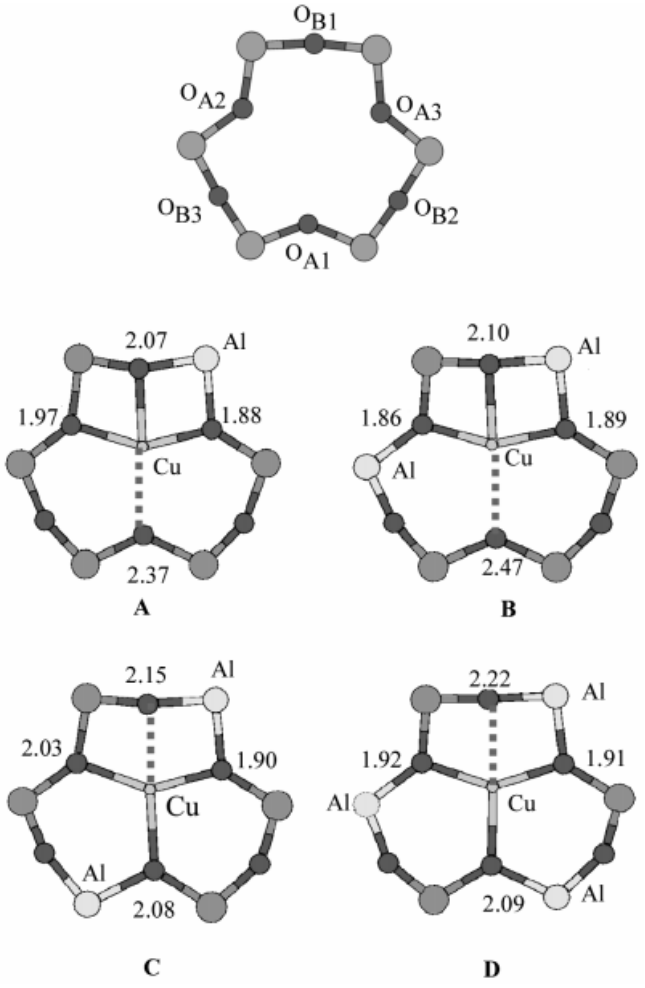

Figure 6. Calculated structures of Cu^{II} in the trigonal six-membered ring site; Cu−O distances are given in Å; cluster A contains only one Al, clusters B, C contain two Al, while three Al are present in cluster D; the coordination geometry of Cu^{II} is fourfold planar; one can clearly distinguish the two coordination modes in the six-membered ring: clusters A, B on the one hand and clusters C, D on the other hand; clusters A, B represent B3LYP-DFT structures, while cluster C, D contain a CASPT2-optimized Cu−O_{B1} bond

energies are calculated between 9500 and 15400 cm^{-1}, in good agreement with the experimental ligand field bands. The energy term diagram is shown in Figure 4C. A new assignment of the experimental ligand field bands is proposed, as shown in Table 3.

One can also see from Figure 6 that the cation shows a strong preference for coordination to oxygen atoms bound to Al rather than Si. This also means that the aluminum distribution may thoroughly influence the coordination environment of Cu^{II}. Two distinct fourfold coordination modes could be distinguished, depending on the number and relative positions of Al in the six-membered ring. In clusters A and B, the Cu−O_{B1} distance is much shorter than Cu−O_{A1}. On the other hand, Cu−O_{A1} is shorter than Cu−O_{B1} in rings C and D, due to the introduction of a second Al next to O_{A1}. The two coordination modes can also clearly be distinguished by looking at the calculated *g* factors. The $g_{//}$ value is systematically lower (2.31−2.33) for

the clusters A and B, than for the other group with clusters C and D (2.39−2.41). Based on the close correspondence between the calculated *g* factors and the experimental ESR signals of zeolite A and Y, a new interpretation of these signals is proposed. The occurrence of two ESR signals in zeolite Y as opposed to only one signal in zeolite A can be attributed to the higher Si/Al ratio in the former zeolite. In zeolite A, with an Si/Al ratio of 1, only the ring shown in Figure 6D can occur, explaining the single ESR signal with $g_{//} = 2.38$. On the other hand, rings with 1, 2 or 3 Al (all structures in Figure 6) can occur in zeolite Y, which leads to the two ESR signals. This new interpretation is corroborated by the experimental ESR signals obtained for Cu^{II}−ZK4 (with Si/Al > 1).[28,97] Also here, two ESR signals are observed, while only one six-membered ring site is present. On the other hand, the rather high $g_{//}^{(2)}$ value observed in the Cu^{II}−zeolite X remains puzzling.

Finally, we should remark that for clusters with more than 1 Al, there are different structural minima for Cu^{II} in the six-membered ring. The energy barriers for going from one minimum to another are low, which indicates that at room temperature Cu^{II} is likely to undergo a hopping process between the different minima. This also explains why the actual minima are not detected on the time-scale of an XRD measurement.

As a next step, the DFT/CASPT2 approach was applied to investigate how the coordination of Cu^{II} in the six-membered ring is influenced when an external ligand is adsorbed at the Cu^{II} ion.[29] The structures of the six-membered rings were reoptimized with B3LYP-DFT in the presence of one NH_3 or H_2O ligand. Adsorption on Cu^{II} in the two coordination modes in the six-membered ring may be compared by considering clusters B and D in Figure 6. For both clusters, it is found that the weakest of the four Cu−O bonds is partially given up upon adsorption of NH_3 or H_2O, and a new strong bond is formed with the extra-lattice ligand instead. This means that for cluster B, the $Cu-O_{A1}$ bond is partially relaxed, while in cluster D, the CuO_{B1} bond is relaxed. When the binding energies were calculated, it was found that adsorbed NH_3 systematically gives a stronger bond than H_2O.

The ligand field spectra of the clusters with external ligands were compared to those of the naked Cu^{II} clusters. The CASPT2 excitation energies of the adsorption complexes are calculated at a lower energy than that of the Cu^{II} clusters without adsorbent. This is in agreement with experimental observations; it is known that the partially hydrated or ammoniated Cu^{II}−Y samples are characterized by a ligand field band in the range 10500−12500 cm^{-1}, somewhat lower than the ligand field band for fully dehydrated Cu^{II}−Y.[29,121] It has indeed been proposed in the literature that the Cu^{II} species in these partially saturated samples are complexes with Cu^{II} coordinated to three lattice oxygen atoms of the six-membered ring site and one external ligand.[41,121] On the other hand, a trigonal bipyramidal complex with Cu^{II} coordinating to three oxygen atoms of the six-membered ring and two axial H_2O or NH_3 molecules has also been suggested.[101] So far, clusters with more than one external ligand have not been studied with the ab initio approach.

5. The Siting of Cu^{II} Ions in Mordenite

5.1 XRD

According to the best of our knowledge, XRD data on fully dehydrated Cu^{II}−mordenite are not available yet. Therefore, other XRD data are often consulted to obtain a first indication of possible coordination sites of Cu^{II}. In partially dehydrated Cu^{II}−mordenite,[122] three sites for Cu^{II} were determined. In site A (see Figure 1C) the Cu^{II} ions are not only coordinated to six lattice oxygen atoms of the eight-membered ring, but also to two water molecules. A second occupied site is the six-membered ring in the twelve-membered ring channel (site E), where the Cu^{II} ion is coordinated to four lattice oxygen atoms of the six-membered ring. The last and least occupied site is site D, where Cu^{II} is bound to three oxygen atoms of the circular eight-membered ring. It can, however, not be excluded that the Cu^{II} ion further migrates to other cation sites upon complete dehydration.

Most of the interpretations of the siting of Cu^{II} in mordenite are based on the much earlier XRD results of dehydrated Ca^{II} mordenite.[123] Four sites are occupied by Ca^{II}. Ca^{II} ions are first found in site A, where this ion is coordinated to six lattice oxygen atoms in C_{2h} symmetry. The second exchange site which is occupied by Ca^{II} is site E, where Ca^{II} is coordinated to four lattice oxygen atoms. A smaller portion of the Ca^{II} ions is located in the boat-shaped site in the eight-membered ring channel of the zeolite. This site is composed of a non-planar six-membered ring (site C) in between two bent five-membered rings. Finally, Ca^{II} ions were also found in site D. It should, however, be noted that the ion radius for Cu^{II} is much smaller than that of Ca^{II}, which can result in different preferential sites for dehydrated Cu^{II}− and Ca^{II}−mordenite. Moreover, it can also be expected that transition metal cations react differently with the zeolite than the closed shell alkaline-earth cations. Any interpretation of the spectroscopic signals in Cu^{II}−mordenite on the basis of these two available XRD studies is therefore speculative.

5.2 ESR and DRS Studies

In the first ESR studies of Cu^{II}-exchanged mordenite, two types of Cu^{II} cations, both in an axial environment, were detected, with $g_{//}^{(1)} = 2.32$ and $g_{//}^{(2)} = 2.27$ (as also reported in Table 2).[124,125] The two coordination environments were described as either four-coordinated square-planar (characterized by $g_{//}^{(2)} = 2.27$) or five-coordinated square-pyramidal (characterized by $g_{//}^{(1)} = 2.32$). An investigation of the Cu^{II} reducibility provided additional information on the coordination of these ions. The Cu^{II} ions in the close to square-planar coordination are readily reduced by CO at 400 °C, while the five-coordinated Cu^{II} ions are more stable to reduction by CO. It was therefore suggested that

the five-coordinated Cu^{II} ion compensates for the two elemental charges of the mordenite lattice and has no additional link to extra-lattice oxygen ligands. The reduction process for the latter species must involve the abstraction of an O^{2-} anion from the zeolitic framework and should prove difficult. Finally, the accessibility of the Cu^{II} species was examined. It was shown that both types of Cu^{II} ions interact with cation-radicals of large molecules such as benzene and *o*-xylene via a dipole−dipole interaction, implying that they must be located in sites that are accessible from the main channel.

Sass and Kevan[126] studied the coordination of Cu^{II} in mordenite in the presence of adsorbed molecules. Due to the very low Cu^{II} loadings (1 Cu^{II} per 30 unit cells), they observed only one ESR signal in CuNa−, CuK− and CuCa−mordenite, with $g_{//}^{(1)} = 2.32-2.33$. This Cu^{II} species was assigned to Cu^{II} in site A.

De Tavernier and Schoonheydt observed the same two Cu^{II} signals with ESR as Kucherov, and found that their relative intensities are dependent on the Cu^{II} loading, the Si/Al ratio and co-exchanged cations.[20,30,31,127] At small Cu^{II} loadings, only the ESR signal with $g_{//}^{(1)} = 2.33$ is detected. In the DRS spectrum of these samples, a ligand field band with maximum intensity at 13700 cm^{-1} is observed. In contrast with the DRS spectra of zeolite Y, the individual transitions of this band are not resolved. When the Cu^{II} loading is increased, the second signal ($g_{//}^{(2)} = 2.27$) also becomes apparent in the ESR spectrum. This goes along with a broadening of the DRS ligand field band. An interpretation of these combined DRS/ESR data of Cu^{II}−mordenite was provided on the basis of AOM calculations.[127] According to this interpretation only site A is occupied at low Cu^{II} exchange levels, in agreement with the assignment of Kevan. The weak coordination with six oxygen atoms at this site gives rise to the ESR signal with a $g_{//}^{(1)}$ value of 2.32. At higher copper loadings, a second exchange site, i.e. site E, becomes occupied. The fourfold Cu−oxygen coordination at this site was held responsible for the second ESR signal with $g_{//}^{(2)} = 2.27$.

Carl and Larsen[128,129] also decomposed the ESR spectrum of CuNa−mordenite into two axial signals, but with different parameters $g_{//} = 2.33$, $A_{//} = 164\ 10^{-4}\ cm^{-1}$ and $g_{//} = 2.34$, $A_{//} = 121\ 10^{-4}\ cm^{-1}$. While the first signal is in good correspondence with that found by de Tavernier, the second signal has an exceptionally low value of $A_{//}$ ($121\ 10^{-4}\ cm^{-1}$). A third ESR signal was also present, but its parameters could not be resolved.

The siting of Cu^{II} in various Si-rich zeolite matrices, including mordenite, has been studied extensively by Wichterlová et al.[23−25] They combined conventional ESR measurements with Cu^{I} luminescence and IR studies of adsorbed NO on Cu^{II} and also studied the reducibility of the Cu^{II} ions. It was assumed that the Cu^{I} siting and distribution reflect those of the Cu^{II} ion. As shown in Table 5, four main coordinations of the Cu ions, common in ZSM-5, mordenite, erionite, and zeolite beta, were distinguished. These authors concluded that the Cu^{II} siting in high silica zeolites is essentially controlled by the local Si−Al sequences in the framework, in agreement with the earlier suggestions of Kucherov.[124,125] Cu^{II} characterized by $g_{//}^{(1)} = 2.32$ is preferentially located in the close vicinity of two framework aluminum atoms. Here it obtains the square-pyramidal oxygen coordination. The Cu^{II} ions are strongly bound to the zeolite lattice and they are not easily reduced. A second type of Cu^{II}, characterized by a $g_{//}^{(2)}$ value of 2.27, has a square-planar oxygen coordination and is adjacent to a single aluminum atom. This site is easily reduced and was suggested to be responsible for the high and stable activity of Cu−zeolites in NO decomposition.[130,131] The possibility of an extra-framework oxygen ligand (O^- or OH^-) was, for the latter site, also considered.

From an FTIR study of the framework T−O−T vibrations, Wichterlová et al. also showed that the bonding of Cu^{II} (or other divalent cations) to the framework oxygen atoms causes local deformations in the zeolite framework.[79] Upon reduction of Cu^{II} to Cu^{I} or the adsorption of a ligand on the Cu^{II} ion, the band shifted to higher wavenumbers, indicating some relaxation of the framework.

5.3 Ab initio Studies of the Siting of Cu^{II} in Mordenite

Pierloot et al.[30,31] also performed ab initio calculations in order to interpret the two ESR signals of Cu^{II} in mordenite. Cluster models of several cation exchange sites in mordenite were constructed, based on the XRD structure of Ca^{II}−mordenite. These clusters consist of the ring systems in Figure 2 terminated by OH groups or hydrogen atoms. The considered sites were site A, as a representative of an oxygen eight-membered ring site, and sites E and C (see Figures 1C and 2).

The structure and spectroscopic features of Cu^{II} on these cation exchange sites were calculated with the DFT/CASPT2 approach, using a similar strategy as described in section 4.4. The effect of the aluminum distribution on the coordination environment, spectroscopic features and siting

Table 5. Spectroscopic signatures of Cu^{II} as established by Wichterlová et al.:[23−25] Cu^{+} emission wavelengths, IR frequencies of Cu^{2+}−NO, and ESR parameters of Cu^{2+}

Cu site	Cu^{+} emmision [nm]	Cu^{2+}−NO [cm^{-1}]	$g_{//}$	Al	Cu^{2+} coordination
Cu-I	450	1921 (1909)	2.31	Al pairs	square-pyramidal
Cu-II	480	1912	2.33	Al pairs	square-pyramidal
Cu-III	510	1906	−		
Cu-IV	540	1896	2.28	single Al	square-planar

of Cu^{II} was examined in detail. The calculated spectroscopic features were confronted with the experimental DRS and ESR data in order to understand the siting of Cu^{II} in mordenite.

The geometry optimizations of site-A clusters indicate that the Cu^{II} ion cannot acquire a fourfold coordination environment in this site. The distortions induced by Cu^{II} are insufficient to realize an optimal fourfold oxygen coordination. Eight-membered rings are simply too large to supply Cu^{II} with the desired planar oxygen four-coordination. This was also shown by a molecular modeling study of the coordination of Cu^{II} in mordenite.[132] As a consequence of the weak coordination, the obtained ligand field is not strong enough to explain the observed spectroscopic features of Cu^{II}−mordenite (the CASPT2 excitation energies remain below 10000 cm^{-1}). Therefore, the eight-membered ring sites in mordenite will be excluded from the following considerations.

As a next step, the coordination of Cu^{II} in the cluster models of site E and site C was studied. The geometry optimizations show that Cu^{II} can obtain a strong fourfold coordination environment in the planar rings of these sites, i.e. in the six-membered ring of site E and in the planar five-membered ring of site C. Let us first look at the results for site E. As for the trigonal six-membered ring site, two coordination modes can be distinguished in the six-membered ring of site E, depending on the relative positions of Al. A representative cluster of each of these two coordination modes is represented in Figure 7. Coordination mode I is realized if Al is present at the central positions in the six-membered ring. Then, an almost perfect square-planar coordination is obtained (see Figure 7), with four Cu−O distances of around 2 Å. This strong coordination gives rise to a ligand field spectrum at high energy (and is in agreement with experimental results), and axial g factors with a $g_{//}$ value around 2.27. On the other hand, more distorted coordination environments are present if Al is placed at less central positions, mode II in Figure 7. Cu^{II} forms a bond with one of the less central oxygen atoms due to the preference of Cu^{II} for coordination with oxygen atoms bound to Al. As can be seen from Figure 7, this results in a planar four-coordination with one rather large O−Cu−O angle. This distortion of the coordination environment slightly weakens the strength of the ligand field, resulting in higher characteristic $g_{//}$ values ($g_{//}$ = 2.30−2.32) for coordination mode II as compared with mode I.

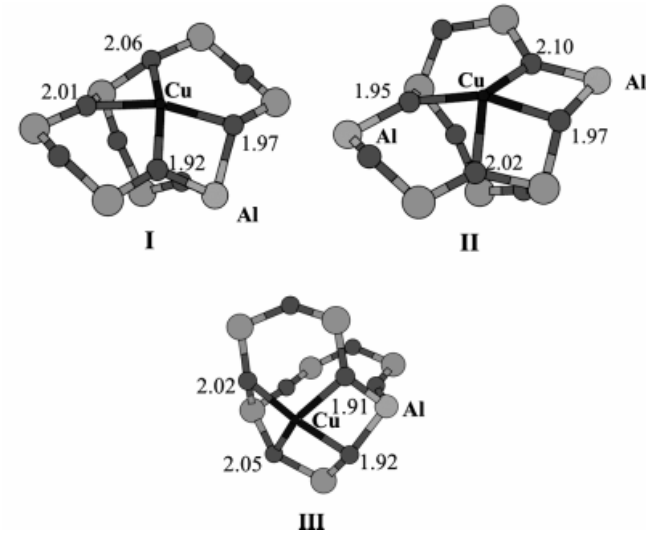

Figure 7. The representative coordination modes for Cu^{II} in mordenite; cluster I represents Cu^{II} in site E where one Al is present at a central position; the Cu^{II} ion obtains a planar fourfold coordination environment; cluster II represents Cu^{II} in site E with two Al at non-central positions; Cu^{II} is present in an irregular fourfold coordination environment; cluster III represents Cu^{II} in the planar five-membered ring in the main channel, where this ion obtains a fourfold pyramidal coordination; the Cu−O distances are given in Å

At site C, it was found that Cu^{II} acquires a pyramidal four-coordination in the planar five-membered rings, coordination mode III in Figure 7. Due to the small size of the five-membered ring, the Cu^{II} ion is located slightly above the plane of the oxygen atoms, in the main channel of mordenite. This pyramidal coordination is also characterized by $g_{//}$ = 2.27, and this third coordination mode can therefore not be distinguished from mode I in site E.

As one can see, the calculated g factors characterizing coordination mode I, II and III are in good agreement with the experimental ESR spectra. The ESR signal with $g_{//}^{(1)}$ = 2.33 is assigned to Cu^{II} in coordination mode II, while the second signal with $g_{//}^{(2)}$ = 2.27 can be assigned to Cu^{II} ions in coordination mode I and/or III. Additional considerations must be taken into account in order to explain the order in which the two ESR signals appear; first, it may be expected that the Cu^{II} ions prefer rings in which two Al are present above rings containing only one Al, due to electrostatic effects. Second, the rule of Takaishi for the ordered aluminum distribution in mordenite was invoked.[133][134] According to this rule, the five-membered rings in mordenite can never contain more than one Al. This also implies that not all six-membered rings with two Al in site E and C can occur (as linking five-membered rings forms them). Six-membered rings with 2 Al at central positions cannot be formed in mordenite; 2 Al must be placed at the non-central positions.

The following interpretation of the siting of Cu^{II} ions in mordenite is then proposed: at low Cu^{II} loadings, the Cu^{II} ions are found at the preferential sites, that is in rings with two aluminum atoms. Takaishi's rule excludes those aluminum distributions that might have provided Cu^{II} with a regular square-planar coordination in a ring containing 2 Al. As such, only coordination mode II (see Figure 7) is realized at the lowest Cu^{II} loadings, leading to only one ESR signal with $g_{//}$ = 2.33. The number of vacant six-membered rings decreases when the Cu^{II} loading increases. Therefore, rings with 1 Al also become occupied at higher Cu^{II} loadings, so that the more regular square-planar or square-pyramidal coordination modes in the planar five- and six-membered ring in the main channel are also formed. This gives rise to the second ESR signal, characterized by $g_{//}$ = 2.27. We remark that the Cu^{II} ions are located in the main channel of mordenite, and as such they are

well accessible for adsorbing molecules, in agreement with ESR results.[124]

Finally, the charge compensation of Cu^{II} in rings with only 1 Al was examined. In the literature, it is often suggested that Cu^{II} ions in the vicinity of only 1 Al are coordinated to an extra-lattice OH^- ligand in order to compensate for the local positive charge.[23,70,128,135] To test this hypothesis, additional calculations were performed for clusters with 1 Al, where Cu^{II} is also coordinated to OH^-. The optimized structures show that the Cu^{II} ion is in a planar threefold coordination environment. The Cu^{II} ion is moved outside the plane of the zeolite ring and remains coordinated to only two of the lattice oxygen atoms (the ones bound to Al) and the OH^- group. The latter bond has an unusually short Cu−O distance. This trigonal coordination is very unusual in the inorganic coordination chemistry of Cu^{II}. The $g_{//}$ factors characterizing this coordination (around 2.40) are much higher than the experimentally observed ESR signals. It is concluded that the $(Cu-OH)^+$ species are not present in the Cu^{II}−mordenite samples considered here. Charge compensation therefore only proceeds via Al in the lattice. In the case of Cu^{II} in rings with only 1 Al, this implies that charge compensation is also realized by Al in a next shell of the zeolite structure.

6. Concluding Remarks

The present work demonstrates that the structure and spectroscopic properties of transition metal ions in zeolites can successfully be explained by means of cluster model calculations using a combined DFT/CASPT2 treatment. Accurate structural information about the coordination of the transition metal ion and the distortions of the zeolite framework due to the metal adsorption is obtained from the partial geometry optimizations based on DFT. The spectroscopic features of the cluster models were calculated by means of the CASPT2 method. The ligand field excitation energies were predicted with an accuracy of less than 1000 cm^{-1}, while the ESR g factors were calculated with an accuracy of 0.03.

The DFT/CASPT2 approach allows a thorough investigation of the role of the Al distribution on the coordination environment and siting of the transition metal ion, which turns out, plays a crucial role in the cation−zeolite interaction. The main disadvantage of the cluster model approach could be the neglect of the effect of the rest of the zeolite crystal on the coordination environment of the transition metal ion. One may wonder whether restricted model clusters can correctly describe the cation exchange sites in the real zeolite matrix. However, the excitation energies and g factors crucially depend on the structure of the cluster model. The close correspondence between the experimental and calculated spectroscopic features therefore indirectly confirms the high quality of the DFT structures. The fact that the coordination environment and spectroscopic properties of transition metal ions in the considered zeolites can be described by the relatively small cluster models used in this work is an indication that they are essentially only dependent on the nearest neighbors of the cation. It would be interesting to examine the effect of the wider zeolite environment by using a QM/MM embedding procedure. In this method, the quantum mechanical (QM) description of the cluster is coupled with a classical description (with molecular modeling, MM) of the interactions between the cluster and its further environment.[58−60]

The study of the coordination of Cu^{II} in zeolite A, Y, ZK4 and mordenite has led to a new and profound insight in the Cu^{II}−zeolite interaction, which can be summarized by the following three rules:

(1) The presence of Cu^{II} in cation exchange sites in zeolites causes local distortions of the zeolite framework. The driving force for these structural deformations is the tendency of Cu^{II} to attain a four-coordinate square-planar coordination to the lattice oxygen atoms. This can be rationalized by means of molecular orbital theory; in a square-planar environment, Cu^{II} can maximize the σ interaction between the $Cu(3d_{x^2-y^2})$ orbital and the oxygen ligands. The Cu−O binding thus has a partially covalent character.

(2) Framework aluminum atoms strongly influence the coordination environment of Cu^{II}, since the cation preferentially coordinates to lattice oxygen atoms bound to Al. As there are different possible Al distributions in one site (for zeolites with Si/Al > 1), this can lead to different coordination modes for Cu^{II} in one site.

(3) Planar five- and six-membered rings are the ideal sites to accommodate the Cu^{II} ion, as the planar fourfold coordination is most easily achieved in these rings. Larger or twisted rings are avoided.

In the future, it will be interesting to examine and compare the reaction mechanism and reactivity of these transition metal ion centers for the N_2O and NO_x decomposition reactions.

Finally, the performance of the DFT/CASPT2 approach can also be compared to previous theoretical calculations of transition metal ions in zeolites, which were based on crystal or ligand field theory.[20,50−55] Whereas the crystal/ligand field calculations essentially had a rationalizing role, the current DFT/CASPT2 approach has proven to have a predictive value. As a first example, the DFT/CASPT2 calculations have revealed large local distortions of the zeolite structure due to the presence of the transition metal ion. These local deformations of the zeolite in the presence of divalent cations were already decided from IR spectroscopy experiments, where a shift of the framework T−O−T stretching vibrations is observed upon complexation with the cations,[79,80] and from ESEEM and ^{27}Al NMR spectroscopy experiments.[115] In this respect, the DFT structures offer detailed structural information about these distortions which has, so far, been inaccessible to experiment. Secondly, our new interpretation of the ESR signals of Cu^{II} in zeolite A and Y suggested the presence of two ESR signals in a related zeolite, namely Cu^{II}−ZK4. The subsequent ESR experiments on this zeolite indeed confirmed this prediction.

The new ab initio interpretations differ quite significantly from many previous ligand field results on the coordination

of Cu^{II} in zeolites. On the other hand, some of the main ideas of ligand field theory apparently survive. The predominant orbitals that constitute the complete basis of the whole ligand field framework are the metal d orbitals. And these very same orbitals play a crucial role in the construction of the complete active space of the ab initio work. The unique role of the $d_{x^2-y^2}$ orbital in the stabilization of the four-coordinate square-planar coordination is completely in line with simple ligand-field predictions.

Acknowledgments

This investigation has been supported by grants from the Flemish Science Foundation (FWO) and from the Concerted Research Action of the Flemish Government (GOA). M. G. thanks the Institute for the Promotion of Innovation by Science and Technology in Flanders (IWT) for a research grant.

[1] *Atlas of Zeolite Structure Types*, Structure Commission of the International Zeolite Association (IZA-SC), http://www.iza-structure.org/databases
[2] M. Hartmann, L. Kevan, *Chem. Rev.* **1999**, *99*, 635.
[3] B. M. Weckhuysen, R. R. Rao, J. A. Martens, R. A. Schoonheydt, *Eur. J. Inorg. Chem.* **1999**, 565.
[4] M. Iwamoto, H. Furukawa, Y. Mine, F. Uemura, S. Mikuriya, S. Kagawa, *J. Chem. Soc., Chem. Commun.* **1986**, 1273.
[5] M. Iwamoto, H. Yahiro, K. Tanda, N. Mizuno, Y. Mine, S. Kagawa, *J. Phys. Chem.* **1991**, *95*, 3727.
[6] Y. Li, W. K. Hall, *J. Phys. Chem.* **1990**, *94*, 6145.
[7] Y. Li, W. K. Hall, *J. Catal.* **1991**, *129*, 202.
[8] J. Valyon, W. K. Hall, *Catal. Lett.* **1993**, *19*, 109.
[9] M. Anpo, M. Matsuoka, K. Hanou, H. Mishima, H. Yamashita, H. H. Patterson, *Coord. Chem. Rev.* **1998**, *171*, 175.
[10] H. Esemann, H. Förster, *J. Mol. Struct.* **1999**, *482/483*, 7.
[11] Y. Li, J. N. Armor, *Appl. Catal. B: Environ.* **1992**, *1*, 21.
[12] F. Kapteijn, J. Rodriguez-Mirasol, J. A. Moulijn, *Appl. Catal. B: Environ.* **1996**, *9*, 25.
[13] F. Kapteijn, G. Marbán, J. Rodriguez-Mirasol, J. A. Moulijn, *J. Catal.* **1997**, *167*, 256.
[14] M. Shimokawabe, K. Hirano, N. Takezawa, *Catal. Today* **1998**, *45*, 117.
[15] A. Dandekar, M. A. Vannice, *Appl. Catal. B: Environ.* **1999**, *22*, 179.
[16] M. Shelef, *Chem. Rev.* **1995**, *95*, 209.
[17] H. Mishima, K. Hashmoto, O. Takehiko, M. Anpo, *Appl. Catal. B: Environ.* **1998**, *19*, 119.
[18] G. Centi, F. Razzini, A. Galli, *Res. Chem. Intermed.* **1998**, *24*, 541.
[19] E.-Y. Choi, I.-S. Nam, Y. G. Kim, *J. Catal.* **1996**, *161*, 597.
[20] R. A. Schoonheydt, *Catal. Rev. Sci. Eng.* **1993**, *35*, 129.
[21] L. Kevan, *Rev. Chem. Intermed.* **1987**, *8*, 53.
[22] C. J. J. den Ouden, R. A. Jackson, C. R. A. Catlow, M. F. M. Post, *J. Phys. Chem.* **1990**, *94*, 5286.
[23] J. Dědeček, Z. Sobalík, Z. Tvarůžková, D. Kaucký, B. Wichterlová, *J. Phys. Chem.* **1995**, *99*, 16327.
[24] B. Wichterlová, Z. Sobalík, A. Vondrová, *Catal. Today* **1996**, *29*, 149.
[25] B. Wichterlová, Z. Sobalík, J. Dědeček, *Catal. Today* **1997**, *38*, 199.
[26] K. Pierloot, A. Delabie, C. Ribbing, A. A. Verberckmoes, R. A. Schoonheydt, *J. Phys. Chem. B* **1998**, *102*, 10789.
[27] K. Pierloot, A. Delabie, A. A. Verberckmoes, R. A. Schoonheydt, in *Density Functional Theory, a Bridge between Chemistry and Physics* (Eds.: P. Geerlings, F. D. Proft, W. Langenaeker), VUB University Press, Brussels, **1999**, pp. 169−188.
[28] K. Pierloot, A. Delabie, M. H. Groothaert, R. A. Schoonheydt, *Phys. Chem. Chem. Phys.* **2001**, *3*, 2174.
[29] A. Delabie, K. Pierloot, M. H. Groothaert, B. M. Weckhuysen, R. A. Schoonheydt, *Micropor. Mesopor. Mat.* **2000**, *37*, 209.
[30] A. Delabie, K. Pierloot, M. H. Groothaert, B. M. Weckhuysen, R. A. Schoonheydt, *Phys. Chem. Chem. Phys.*, in press.
[31] A. Delabie, M. H. Groothaert, R. A. Schoonheydt, K. Pierloot, in *Proceedings of the 13th international zeolite conference* (Eds.: A. Galarneau, F. D. Renzo, F. Fajula, J. Vendrine), Elsevier Science, **2001**.
[32] M. H. Groothaert, R. A. Schoonheydt, A. Delabie, K. Pierloot, in *Unique metal Ion Structures in Solid Matrices. From Science to Application* (Eds.: B. Wichterlová, A. T. Bell), Kluwer Academic Publishers, Dordrecht, **2001**, pp. 205−219.
[33] W. Loewenstein, *Am. Miner.* **1942**, *39*, 92.
[34] R. J. Faber, M. T. Rogers, *J. Am. Chem. Soc.* **1959**, *81*, 1849.
[35] J. T. Richardson, *J. Catal.* **1967**, *9*, 172.
[36] U. Krüerke, P. Jung, *Z. Phys. Chem. (Frankfurt)* **1968**, *58*, 53.
[37] H. B. Slot, J. L. Verbeek, *J. Catal.* **1968**, *12*, 216.
[38] D. Mikheikin, V. A. Shvets, V. B. Kazanskii, *Kinet. Katal.* **1968**, *29*, 1395.
[39] C. Naccache, B. Taarit, *Chem. Phys. Lett.* **1971**, *11*, 11.
[40] J. Turkevich, Y. Ono, J. Soria, *J. Catal.* **1972**, *25*, 44.
[41] E. F. Vansant, J. H. Lunsford, *J. Phys. Chem.* **1972**, *76*, 2860.
[42] E. F. Vansant, *Recl. Trav. Chim.* **1973**, *11*, 1152.
[43] D. Goldfarb, in *Spectroscopy of transition metal ions on surfaces* (Eds.: B. M. Weckhuysen, P. Van Der Voort, G. Catana), Leuven University Press, **2000**, pp. 93−133.
[44] C. C. Chao, J. H. Lunsford, *J. Phys. Chem.* **1972**, *57*, 2890.
[45] A. A. Verberckmoes, B. M. Weckhuysen, J. Pelgrims, R. A. Schoonheydt, *J. Phys. Chem.* **1995**, *99*, 15222.
[46] A. A. Verberckmoes, B. M. Weckhuysen, R. A. Schoonheydt, K. Ooms, I. Langhans, *Anal. Chim. Acta* **1997**, *348*, 267.
[47] A. A. Verberckmoes, B. M. Weckhuysen, R. A. Schoonheydt, *Stud. Surf. Sci. Catal.* **1997**, *105*, 623.
[48] J. Dědeček, B. Wichterlová, *J. Phys. Chem. B* **1999**, *103*, 1462.
[49] P. Gallezot, Y. B. Taarit, B. Imelik, *J. Catal.* **1972**, *26*, 295.
[50] J. Texter, D. H. Storme, R. G. Herman, K. Klier, *J. Phys. Chem.* **1977**, *81*, 333.
[51] K. Klier, P. J. Hutta, R. Kellerman, *ACS Symp. Ser.* **1977**, *40*, 108.
[52] D. H. Storme, K. Klier, *ACS Symp. Ser.* **1980**, *135*, 155.
[53] D. Packet, R. A. Schoonheydt, *ACS Symp. Ser.* **1988**, *368*, 203.
[54] R. A. Schoonheydt, *Acad. Analecta* **1987**, *49*, 3.
[55] R. A. Schoonheydt, *J. Phys. Chem. Solids* **1989**, *50*, 523.
[56] A. A. Verberckmoes, R. A. Schoonheydt, A. Ceulemans, A. Delabie, K. Pierloot, *Mat. Res. Proc.* **1999**, 387.
[57] P. J. Carl, S. L. Isley, S. C. Larsen, *J. Phys. Chem. A* **2001**, *105*, 4563.
[58] M. Sierka, J. Sauer, *Faraday Discuss.* **1997**, *106*, 41.
[59] L. Rodriguez-Santiago, M. Sierka, V. Branchadell, M. Sodupe, J. Sauer, *J. Am. Chem. Soc.* **1998**, *120*, 1545.
[60] J. Sauer, *Chem. Rev.* **1989**, *89*, 199.
[61] P. Nachtigall, D. Nachtigallová, J. Sauer, *J. Phys. Chem. B* **2000**, *104*, 1738.
[62] D. Nachtigallová, P. Nachtigall, M. Sierka, J. Sauer, *Phys. Chem. Chem. Phys.* **1999**, *1*, 2019.
[63] W. F. Schneider, K. C. Hass, R. Ramprasad, J. B. Adams, *J. Phys. Chem. B* **1997**, *101*, 4353.
[64] W. F. Schneider, K. C. Hass, R. Ramprasad, J. B. Adams, *J. Phys. Chem. B* **1998**, *102*, 3692.
[65] W. F. Schneider, K. C. Hass, R. Ramprasad, J. B. Adams, *J. Phys. Chem.* **1996**, *100*, 6032.
[66] H. V. Brand, A. Redondo, P. J. Hay, *J. Phys. Chem. B* **1997**, *101*, 7691.
[67] Y. Yokomichi, H. Ohtsuka, T. Tabata, O. Okada, Y. Yokoi, H. Ishikawa, R. Yamaguchi, H. Matsui, A. Tachibana, T. Yamabe, *Catal. Today* **1995**, *23*, 431.
[68] Y. Yokomichi, T. Yamabe, H. Ohtsuka, T. Kakumoto, *J. Phys. Chem.* **1996**, *100*, 14424.
[69] N. U. Zhanpeisov, H. Nakatsuji, H. Hada, M. Anpo, *Catal. Lett.* **1996**, *42*, 173.

[70] B. L. Trout, A. K. Chakraborty, A. T. Bell, *J. Phys. Chem.* **1996**, *100*, 4173.
[71] B. L. Trout, A. K. Chakraborty, A. T. Bell, *J. Phys. Chem.* **1996**, *100*, 17582.
[72] R. J. Blint, *J. Phys. Chem.* **1996**, *100*, 19518.
[73] H. Oka, T. Okada, K. Hori, *J. Mol. Catal. A: Chem.* **1996**, *109*, 51.
[74] N. Tajima, M. Hashimoto, F. Toyama, A. M. El-Nahas, K. Hirao, *Phys. Chem. Chem. Phys.* **1999**, *1*, 3823.
[75] X. Solans-Monfort, V. Branchadell, M. Sodupe, *J. Phys. Chem. A* **2000**, *104*, 3225.
[76] M. J. Rice, A. K. Chakrabotry, A. T. Bell, *J. Catal.* **2000**, *194*, 278.
[77] M. J. Rice, A. K. Chakrabotry, A. T. Bell, *J. Phys. Chem. B* **2000**, *104*, 9987.
[78] J. M. Campos-Martin, A. Guerrero-Ruiz, J. L. G. Fierro, *Catal. Lett.* **1996**, *41*, 55.
[79] Z. Sobalík, Z.; J. Dedecek, I. Ikonnikov, B. Wichterlová, *Microporous Mesoporous Mater.* **1998**, *21*, 525.
[80] Z. Sobalík, Z. Tvarůžková, B. Wichterlová, *J. Phys. Chem. B* **1998**, *102*, 1077.
[81] H. Yamashita, M. Matsuoka, K. Tsuji, Y. Shioya, M. Anpo, M. Che, *J. Phys. Chem.* **1996**, *100*, 397.
[82] C. Lamberti, G. Spoto, D. Scarano, C. Pazé, M. Salvalaggio, S. Bordiga, A. Zecchina, G. T. Palomino, F. D'Acapito, *Chem. Phys. Lett.* **1997**, *269*, 500.
[83] S. Hu, A. Reimer, A. T. Bell, *J. Phys. Chem. B* **1997**, *101*, 1869.
[84] S.-B. Liu, B. M. Fung, T.-C. Yang, E.-C. Hong, C.-T. Chang, P.-C. Shih, F.-H. Tong, T.-L. Chen, *J. Phys. Chem.* **1994**, *98*, 4393.
[85] S.-B. Liu, T.-C. Yang, R.-Y. Lin, E.-C. Hong, T.-S. Lin, *Stud. Surf. Sci. Catal.* **1994**, *84*, 789.
[86] S.-B. Liu, T.-S. Lin, T.-C. Yang, T.-H. Chen, E.-C. Hong, R. Ryoo, *J. Phys. Chem.* **1995**, *99*, 8277v.
[87] H. S. Lee, K. Seff, *J. Phys. Chem.* **1981**, *85*, 397.
[88] I. E. Maxwell, J. J. de Boer, *J. Phys. Chem.* **1975**, *79*, 1874.
[89] R. M. Haniffa, K. Seff, *Microporous Mesoporous Mater.* **1998**, *25*, 137.
[90] N. N. Tikhomiroya, I. V. Nikolaeva, *Zh. Strukt. Khim.* **1969**, *10*, 547.
[91] R. A. Schoonheydt, P. Peigneur, J. B. Uytterhoeven, *J. Chem. Soc., Faraday Trans. 1* **1978**, *74*, 2550.
[92] R. G. Herman, D. R. Flentge, *J. Phys. Chem.* **1978**, *82*, 720.
[93] M. Narayana, L. Kevan, *J. Chem. Soc., Faraday Trans. 1* **1986**, *82*, 213.
[94] M. W. Anderson, L. Kevan, *J. Phys. Chem.* **1987**, *91*, 1850.
[95] T. Ichikawa, L. Kevan, *J. Chem. Soc., Faraday Trans. 1* **1981**, *77*, 2567.
[96] T. Ichikawa, L. Kevan, *J. Am. Chem. Soc.* **1981**, *103*, 5355.
[97] M. W. Anderson, L. Kevan, *J. Phys. Chem.* **1986**, *90*, 3206.
[98] D. R. Flentge, J. H. Lunsford, P. A. Jacobs, J. B. Uytterhoeven, *J. Phys. Chem.* **1975**, *79*, 354.
[99] R. G. Herman, J. H. Lunsford, H. K. Beyer, P. A. Jacobs, J. B. Uytterhoeven, *J. Phys. Chem.* **1975**, *79*, 2388.
[100] I. E. Maxwell, E. Drent, *J. Catal.* **1976**, *41*, 412.
[101] R. G. Herman, *Inorg. Chim. Acta* **1979**, *34*, 119.
[102] J. C. Conesa, J. Soria, *J. Chem. Soc., Faraday Trans. 1* **1979**, *75*, 406.
[103] J. S. Yu, L. Kevan, *J. Phys. Chem.* **1990**, *94*, 7612.
[104] J. C. Conesa, J. Soria, *J. Phys. Chem.* **1978**, *82*, 1847.
[105] J. C. Conesa, J. Soria, *J. Phys. Chem.* **1978**, *82*, 1575.
[106] J. C. Conesa, J. Soria, *J. Chem. Soc., Faraday Trans. 1* **1979**, *75*, 423.
[107] I. R. Leith, C. Kemball, H. F. Leach, *Chem. Commun.* **1971**, 407.
[108] I. R. Leith, H. F. Leach, *Proc. R. Soc. London, Ser A* **1972**, *330*, 247.
[109] J. S. Yu, L. Kevan, *J. Phys. Chem.* **1990**, *94*, 7620.
[110] J. S. Yu, L. Kevan, *J. Phys. Chem.* **1990**, *94*, 5595.
[111] T. Ichikawa, L. Kevan, *J. Am. Chem. Soc.* **1983**, *105*, 402.
[112] T. Ichikawa, L. Kevan, *J. Phys. Chem.* **1983**, *87*, 4433.
[113] J. S. Yu, L. Kevan, *J. Phys. Chem.* **1991**, *95*, 6648.
[114] M. Iwamoto, K. Maruyama, N. Yamazoe, T. Seiyama, *J. Phys. Chem.* **1977**, *81*, 622.
[115] D. Goldfarb, L. Kevan, *J. Magn. Reson.* **1989**, *82*, 270.
[116] D. Goldfarb, K. Zukerman, *Chem. Phys. Lett.* **1990**, *171*, 167.
[117] K. Matar, D. Goldfarb, *J. Phys. Chem.* **1992**, *96*, 3100.
[118] A. Schäfer, H. Horn, R. Ahlrichs, *J. Chem. Phys.* **1992**, *97*, 2571.
[119] K. Pierloot, B. Dumez, P.-O. Widmark, B. O. Roos, *Theor. Chim. Acta* **1995**, *90*, 87.
[120] C. Ribbing, C. Daniel, *J. Chem. Phys.* **1994**, *100*, 6591.
[121] W. De Wilde, R. A. Schoonheydt, J. B. Uytterhoeven, *ACS Symp. Ser.* **1977**, *40*, 132.
[122] M. P. Attfield, S. J. Weigel, A. K. Cheetham, *J. Catal.* **1997**, *170*, 227.
[123] W. J. Mortier, J. J. Pluth, V. J. Smith, *Mater. Res. Bull.* **1975**, *10*, 1037.
[124] A. V. Kucherov, A. A. Slinkin, D. A. Kondrat'ev, T. N. Bondarenko, A. M. Rubinstein, K. M. Minachev, *Zeolites* **1985**, *5*, 320.
[125] A. V. Kucherov, A. A. Slinkin, *Zeolites* **1986**, *6*, 175.
[126] C. E. Sass, L. Kevan, *J. Phys. Chem.* **1989**, *93*, 4669.
[127] S. de Tavernier, R. A. Schoonheydt, *Zeolites* **1991**, *11*, 155.
[128] P. J. Carl, S. C. Larsen, *J. Phys. Chem. B* **2000**, *104*, 6568.
[129] P. J. Carl, S. C. Larsen, *J. Catal.* **1999**, *182*, 208.
[130] B. Wichterlová, J. Dědeček, Z. Sobalík, A. Vondrová, K. Klier, *J. Catal.* **1997**, *169*, 194.
[131] B. Wichterlová, J. Dědeček, A. Vondrová, *J. Phys. Chem.* **1995**, *99*, 1065.
[132] V. Guliants, J. Mullhaupt, J. Newsam, A. Gorman, C. Freeman, *Catal. Today* **1999**, *50*, 661.
[133] T. Takaishi, M. Kato, K. Itabashi, *Zeolites* **1995**, *15*, 21.
[134] T. Takaishi, M. Kato, K. Itabashi, *J. Phys. Chem.* **1994**, *98*, 5742.
[135] M. L. Jacono, G. Fierro, R. Dragone, X. Feng, J. d'Itri, W. K. Hall, *J. Phys. Chem. B* **1997**, *101*, 1979.

Received July 13, 2001
[I01261]